JOURNAL OF Applied Polymer SCIENCE

Functional and Mechanical Properties of Acrylate Elastomer/Expanded Graphite Nanocomposites

Yannan Quan,[1] Ming Lu,[1] Ming Tian,[1,2] Shouke Yan,[1] Zhongzhen Yu,[1] Liqun Zhang[1,2]

[1]College of Material Science and Engineering, Key Laboratory of Beijing City for Preparation and Processing of Novel Polymer Materials, Beijing University of Chemical Technology, Beijing 100029, China

[2]College of Material Science and Engineering, Key Laboratory for Nanomaterials of Ministry of Education, Beijing University of Chemical Technology, Beijing 100029, China

Correspondence to: L. Zhang (E-mail: zhanglq@mail.buct.edu.cn)

ABSTRACT: Expanded graphite (EG) is prepared by microwave irradiation to expandable graphite. A stable aqueous suspension of EG is obtained through dispersing EG into deionized water in the presence of surfactant under ultrasonication. Nanocomposites are prepared by compounding EG aqueous suspension with alkyl acrylate elastomer latex. It is showed that, by the latex compounding method (LCM), EG platelets are finely dispersed in the elastomer matrix. The nanocomposites exhibit remarkable improvements in mechanical properties, wear resistance, and gas barrier property. The prepared compound also shows certain electrical conductivity, but soon loses it after milled on a miller. Meanwhile, a dramatic change in EG network is observed corresponding to the loss of electrical conductivity. © 2013 Wiley Periodicals, Inc. J. Appl. Polym. Sci. 130: 680–686, 2013

KEYWORDS: elastomers; nanocomposites; nanolayers

Received 14 October 2012; accepted 24 February 2013; published online 2 April 2013

DOI: 10.1002/app.39210

INTRODUCTION

Graphite naturally has a nanolayered structure with individual sheets composed of two-dimensional sp^2-hybridized carbon atoms. The exfoliated graphite, also called graphene, is only one atom in thickness. It is known as the thinnest material in the universe. Graphite sheets are well known for its superior mechanical, thermal, and electrical properties,[1–3] and have showed great potentials in functional applications.[4,5] They can provide polymers with competitive properties when a fine dispersion is achieved.[6,7]

The challenges come from the preparation of highly exfoliated graphite sheets and their dispersion in polymer matrices. Currently, an important strategy to exfoliate graphite platelets, also known as the top-down method, is by thermal or chemical exfoliation of graphite oxide.[8–10] There are also the bottom-up method to grow graphene from organic precursors[11,12] and the method of epitaxial growth of graphene on the substrates.[13,14] As far as the preparation of graphite nanosheets/polymer nanocomposites, in our opinion with the presence of the polymer matrix, the first strategy is more applicable.

Expanded graphite (EG), a graphite derivative by converting the natural graphite into intercalated or expandable graphite through chemical oxidation in concentrated H_2SO_4 and HNO_3 acid or other expansion agents, expand rapidly over 200 to 300 times in the c-axis in a thermo shock above 600°C.[15–17] EG shows as worm-like particles with exfoliated graphite flakes. Composed of several stacks of graphite sheet, EG is widely used to enhance the physical properties of polymers.[18–20]

Methods like melt compounding, solution compounding, and *in situ* polymerization have been developed to disperse graphene, carbon nanotubes, and graphite platelets into polymer matrices.[21–23] Ultrasonication is applied to further improve the exfoliation of the graphite nanoplatelets.[24,25] Some work[26] suggest that compared to melt compounding, solution compounding and *in situ* polymerization may endow polymer nanocomposites with higher electrical conductivities and lower percolation thresholds. However, both solution compounding and *in situ* polymerization take complex procedures, consume large amount of solvents, and can only be applied to limited polymers. Latex compounding method (LCM), as a water-mediating method, has been developed as a cost-effective and efficient approach for the preparation of polymer nanocomposites.[27–29]

Acrylate based elastomer (ACM), commonly used in static and dynamic seals, shows strong resistance to hot oil and oxidation. It can work continuously at the temperature of 150°C and intermittently at a limit of 180°C. However, the neat ACM exhibits poor wear resistance and requires reinforcement in mechanical strength.

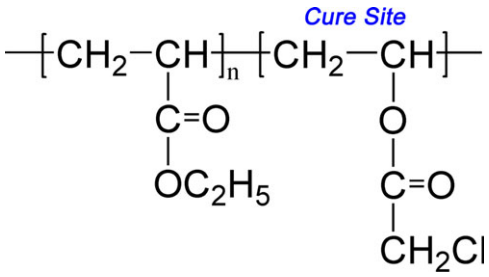

Figure 1. Chemical structure of ACM used in this work. [Color figure can be viewed in the online issue, which is available at wileyonlinelibrary.com.]

It is expected in this work that, by the latex compounding method, the expanded graphite sheets can disperse well in the acrylate based elastomer to prepare nanocomposites with improved mechanical, tribological, and other functional properties. The expanded graphite was obtained by thermal shock of microwave irradiation to the expandable graphite. EG was then dispersed into an aqueous solution of a surfactant to form a stable suspension with the help of ultrasonication. The EG/ACM nanocomposites prepared by the latex compounding method were studied in terms of dispersion of EG platelets, mechanical, and physical properties.

EXPERIMENTAL

Materials

Acrylate elastomer (ACM, AR-100 in the latex form, Suining Qinglong Polyacrylate Manufactory, China) with the brittle temperature of −15°C and the Mooney viscosity of 40ML(1+4)100°C was used as received. The chemical structure of AR-100 ACM is showed in Figure 1. Expandable graphite (KP50, Pingdu Huadong Graphite Processing Factory, China) with an approximate expandable ratio of 250 along the *c*-axis was used. Sodium dodecyl sulfonate (SDS, Beijing Yili Fine Chemical, China) and anhydrous calcium chloride ($CaCl_2$, Beijing Beihua Fine Chemicals) were used as received. Trithiocyanuric acid (TCY, 1,3,5-Triazine-2,4,6-trithiol) was supplied by Taizhou Huangyan Donghai Chemical, and was used as received.

Preparation Procedures

The expanded graphite (EG) was prepared by microwave irradiation to the expandable graphite in a microwave oven (Sanyo EM-183MS1).[30,31] EG was then dispersed in deionized water with the aid of the surfactant SDS. In a typical procedure, the composition ratio of EG, SDS and water is kept at 1 g/5 g/1.5 L. The suspension was subjected to ultrasonic treatment under the power of 1000 W for 2.5 h so that a stable aqueous suspension of EG sheets was obtained.[32]

The acrylate elastomer latex was added to the suspension slowly under vigorous stirring. The mixture was subsequently treated with ultrasonic for another 30 min. After that, the mixture was slowly poured into a 2 wt % $CaCl_2$ aqueous solution under stirring for coagulation. By washing with running water for 5 min and drying in an air-oven at 50°C for 12 h, the EG/ACM coagulated compound was obtained.

Trithiocyanuric acid of 1 phr (part per hundred rubber in weight) was mixed with the obtained compound as the curing agent on a 6-inch two-roll mill. Vulcanization was carried out at 170°C under a pressure of 15 MPa for 90 min (T_{90}, the optimum curing time).

Characterizations

Morphologies of the freeze-fractured surfaces of the vulcanizates and those of the worn surfaces after wear tests were observed with a Hitachi S4700 scanning electron microscope (Hitachi, Japan) operated at an acceleration voltage of 20 kV. The samples for transmission electron microscopy (TEM) were prepared by microtomy, and then investigated with a Tecnai G^2 20 S-TWIN transmission electron microscope (FEI, USA) operated at 200 kV accelerating voltage. Tensile tests were performed with dumbbell-shaped specimens in an Instron tester at 23°C and a crosshead speed of 500 mm/min according to ASTM D412 test method. The strain amplitude dependence of storage modulus was measured on an RPA 2000 rheometer (Alpha Technologies, USA) at 60°C and 1 Hz. Dynamic loss as a function of temperature was measured on a DMTA V dynamic mechanical thermal analyzer (Rheometrics Science Corporation) in tension mode with a heating rate of 3°C/min, a strain amplitude of 0.1%, and a frequency of 1 Hz.

Nitrogen permeation tests were conducted according to ISO 2782 differential-pressure method with a self-made apparatus.[29] The apparatus is set up with a test cell, a gas chromatograph, a test gas controller, and some other associated parts. The test cell, maintaining a constant temperature of 40°C during testing, is divided into a high-pressure side and a low-pressure side by the testing sample. The high-pressure side is supplied with the test gas of nitrogen and maintains a constant pressure of 0.57 MPa during the measurement. The volume of nitrogen gas permeated through the testing sample from the high pressure side to the low-pressure side is measured by the gas chromatograph. The gas permeability coefficient is determined from eq. (1), in which V is the volume of the permeated nitrogen gas during a period of testing time, d is the thickness of the testing sample, s is the gas transmission area, t is the period of testing time, and p is the constant pressure of the test gas on the high-pressure side. Five samples were tested to give the average gas permeability coefficient.

$$P = \frac{V(\mathrm{m}^3) \times d(\mathrm{m})}{s(\mathrm{m}^2) \times t(\mathrm{s}) \times p(\mathrm{Pa})} \quad (1)$$

Volume electrical conductivity was converted from the ohmic resistance measured on a Zheng-Yang QJ-84 ohmmeter by four-probe measurements at 23°C and the relative humidity of 20%, and five specimens were measured for each test. Friction and wear behaviors of the composites were evaluated by using a ring-on-disc tester (Jinan Shijin, China) at 23°C and the relative humidity of 20% with a sliding speed of 0.085 m/s under a normal load of 60 N.[33,34] The specific wear rate ($mm^3\ N^{-1}\ m^{-1}$) is obtained by dividing the wear volume (mm^3) by the product of load (N) × sliding distance (m). Three specimens from each composite were tested. Density of the composite was determined by hydrostatic weighing, and five specimens were tested to give the average.

To all measurements in this work, the mean value is presented as the best estimate for the measured quantities, and the margins of error in the measurement are characterized by the standard deviation of the mean. The propagation of errors is calculated from eq. (2).

$$\text{For} \quad q = f(x, \cdots, z), \quad \Delta q = \sqrt{(f'_x \cdot \Delta x)^2 + \cdots + (f'_z \cdot \Delta z)^2} \quad (2)$$

RESULTS AND DISCUSSION

Dispersion of EG in ACM Matrix

By comparing the EG/ACM composites at the same filler loading, the composite prepared by latex compounding method exhibits far better dispersion of EG platelets than the composite prepared by direct blending, as seen in the TEM and SEM images in Figure 2. We can see that different from the large EG agglomerate particles in the direct blended composite [Figure 2(b,d)], the EG platelets in the composite prepared by LCM [Figure 2(a,c)] shows as more and finer flakes. The nanodispersion of EG platelets was confirmed as revealed by Figure 2(a).

The DMTA result also demonstrates fine dispersion of EG platelets is achieved by the latex compound method. As seen in Figure 3, the composites prepared by LCM exhibit much lower dynamic loss factors than the neat matrix and the composite prepared by direct blending. This result should be attributed to the stronger filler network constructed by the finely dispersed EG platelets in the LCM prepared nanocomposites. Such filler network join in the response to the dynamic outer force together with the rubber molecules during glass-transition, and thus, modify the hysteresis loss of the composites.

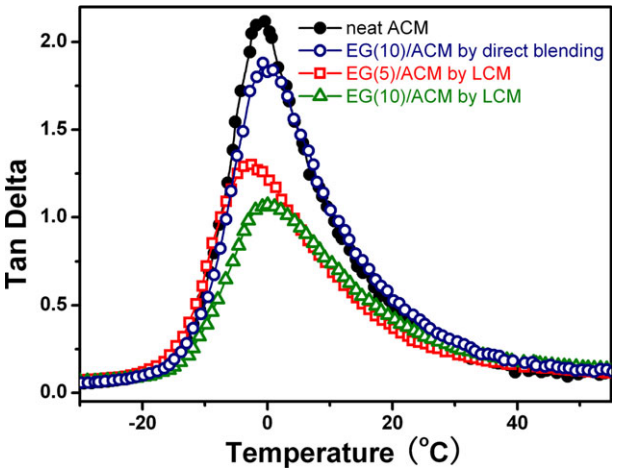

Figure 3. Dynamic loss factors of the neat ACM matrix and the EG/ACM composites prepared by latex compounding method and direct blending. [Color figure can be viewed in the online issue, which is available at wileyonlinelibrary.com.]

Mechanical Properties

Figure 4 displays the stress–strain behaviors of the neat ACM and the EG filled nanocomposites. It is clear that the stress at 100% elongation of the LCM prepared nanocomposite is greatly improved with the increase of EG loading, indicating a high reinforcing effect of the EG platelets.

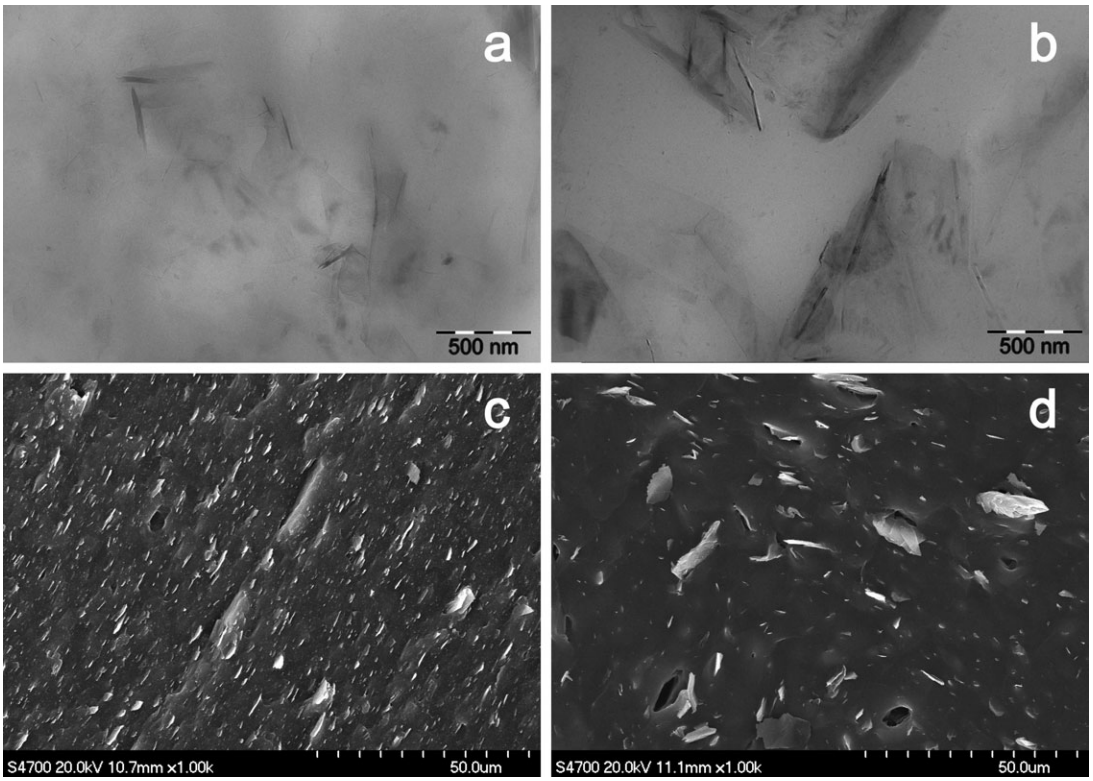

Figure 2. TEM and SEM images of EG(10)/ACM composites prepared by LCM (a, c) and direct blending (b, d), respectively.

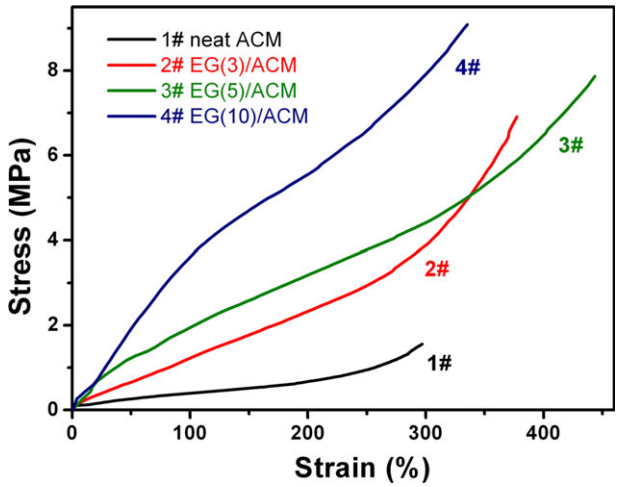

Figure 4. Tensile stress–strain behaviors of neat ACM and EG filled nanocomposites prepared by latex compounding method. [Color figure can be viewed in the online issue, which is available at wileyonlinelibrary.com.]

The aspect ratio of the EG platelets, which greatly influences the properties of the nanocomposites, can alter when under ultrasonication and the shear force during milling. TEM observation to the microtome section of the sample probes only a small area of the nanocomposite thus just for qualitative analysis. In this work, the aspect ratio of EG platelets was analyzed by both Nielsen and Halpin-Tsai models.

Halpin-Tsai model is used to predict the stiffness of the unidirectional composites as a function of the aspect ratio of the filler component.[35–37] The model is described by eqs. (3) and (4), where E, E_f, and E_m represent the moduli of composite, filler and matrix, respectively. Φ_f is the volume fraction of filler, ζ is a function of the aspect ratio of the filler, and η is given in eq. (4). When calculating the elastic modulus of the lamellar-shape reinforcements, $\zeta = 2(2r/d)$[35] $2r/d$ is the aspect ratio of the EG platelets, where r is the radius of the platelet, and d is the thickness of the platelet.

$$\frac{E}{E_m} = \frac{1 + \zeta\eta\Phi_f}{1 - \eta\Phi_f} \tag{3}$$

$$\eta = \frac{E_f/E_m - 1}{E_f/E_m + \zeta} \tag{4}$$

Based on the conversion of eqs. (3) and (4), the aspect ratio value of the reinforcing filler can be determined from eq. (5). Considering that E_f is far larger than E_m in the EG-filled ACM composites, and thus the ratio of E_f/E_m is far bigger than 1, we simply regard $(E_f/E_m - 1)$ is equal to E_f/E_m as a constant. Then eq. (5) can be simplified as eq. (6) for the convenience of calculation. The calculated results are listed in Table I. And the data were compared with the result from the gas permeability measurements in order to get a brief idea of the aspect ratio of the EG platelets in the nanocomposites.

$$\zeta = \frac{E\left(\frac{E_f}{E_m} - \left(\frac{E_f}{E_m} - 1\right)\Phi_f\right) - E_f}{E_m\left(\left(\frac{E_f}{E_m} - 1\right)\Phi_f + 1\right) - E} \tag{5}$$

$$\zeta = \frac{E - E\Phi_f - E_m}{E_f\Phi_f + E_m - E} \cdot \frac{E_f}{E_m} \tag{6}$$

The volume fraction of filler is calculated by the filler weight content (n parts per hundred rubber) from eq. (7), in which V_f and V_c are respectively the volume of the filler and the composite, ρ_c and ρ_f are the densities of the composites (listed in Table I) and the filler (2.266 g/cm[338]).

$$\Phi_f = \frac{V_f}{V_c} = \frac{\rho_c}{\rho_f} \cdot \frac{n}{100 + n} \tag{7}$$

Friction and Wear Properties

Figure 5(a) presents the evolution of apparent friction coefficients of neat ACM and the EG/ACM composites. The nanocomposite prepared by LCM exhibits a stable friction state, while the neat ACM elastomer and the direct blended composite present decrease in friction coefficients. As revealed by visual observations and wear loss analyses, for the neat ACM, the decrease results from the rolling of the scraped bits of rubber particles, and for the direct blended composite, the dissociation of the graphite sheets inside the large agglomerate particles results in the decreased friction coefficient.

Observations to the worn surfaces demonstrate the different wear performances of the composites prepared by the two methods. As seen in Figure 5(b), the nanocomposite prepared by LCM exhibits a rough worn surface with lots of tiny scraped composite grains. For the direct blended composite [Figure 5(c)], however, large pits and holes are observed on a smoother worn surface.

As showed in Table II, compared with the direct blended composite at the same EG loading, the nanocomposite prepared by

Table I. Calculated Results on the Aspect Ratio of the Expanded Graphite Platelets

Filler loading (n) (phr)	E_f[a] (GPa)	E_m[b] (MPa)	E[b] (MPa)	ρ_c (g/cm^3)	Φ_f[c]	ζ	$2r/d$
3	1060	0.24 ± 0.01	1.11 ± 0.01	1.187 ± 0.003	0.0153 ± 0.0001	230 ± 10	115 ± 5
5			1.35 ± 0.04	1.182 ± 0.003	0.0248 ± 0.0001	180 ± 10	90 ± 5
10			2.71 ± 0.13	1.202 ± 0.005	0.0482 ± 0.0002	200 ± 10	100 ± 5

[a]Modulus of graphite is obtained from literature,[39,40] [b]Moduli of the ACM matrix and the filled composites are obtained from derivation of the stress–strain curves in Figure 4, [c]Volume fraction of filler is calculated from weight loading of the filler by eq. (7).

Applied Polymer SCIENCE

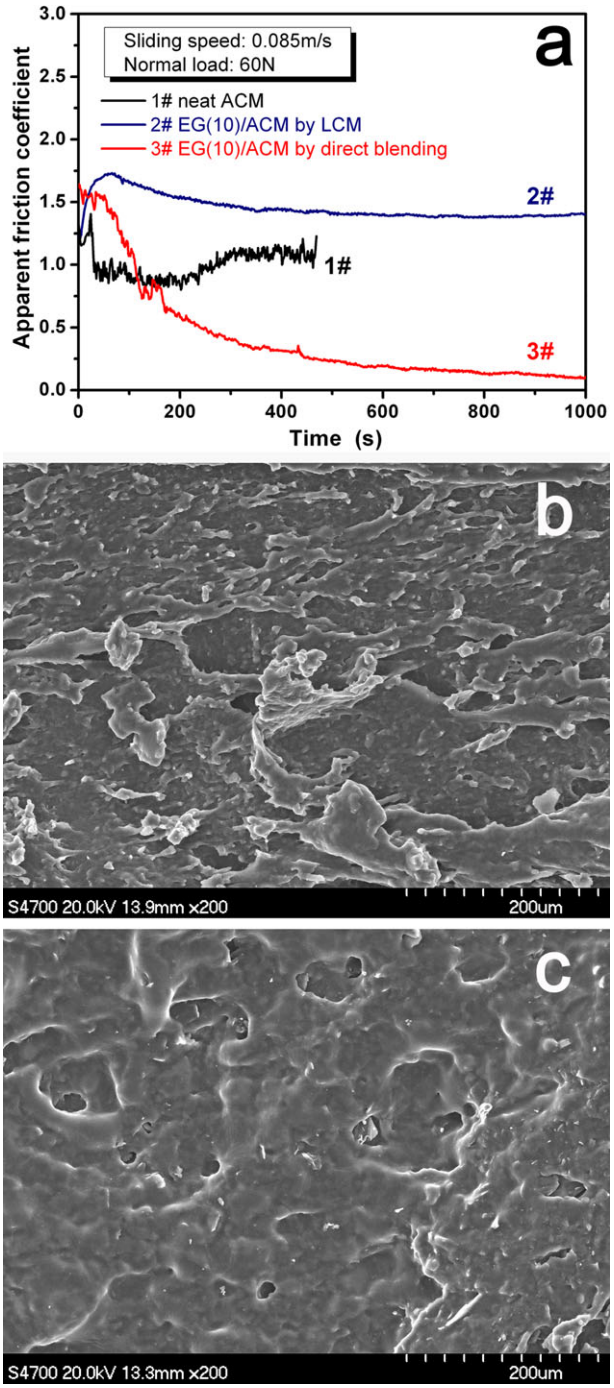

Figure 5. Apparent friction coefficients and worn surfaces of the EG/ACM composites (a is the evolution of apparent fraction coefficients; b and c are the SEM images of the worn surfaces of the EG(10)/ACM composites prepared by LCM and direct blending, respectively). [Color figure can be viewed in the online issue, which is available at wileyonlinelibrary.com.]

LCM exhibits a much lower specific wear rate due to the improved mechanical strength. But, despite the difference in wear rate, we should say that the direct blended composite benefits from the dissociation of the graphite sheets inside the large agglomerate particles in dramatically decreased friction coefficient.

Gas Barrier Properties

Generally, rubbers exhibit relatively lower gas barrier properties compared with plastics because of larger free volume. The gas permeability of a rubber can be modified by the addition of suitable fillers. The EG sheets, with a similar lamellar structure like the layered silicates, are believed to be efficient in maximizing the tortuous paths for a diffusing penetrant. The nitrogen gas permeability coefficients of neat ACM and the EG/ACM nanocomposites were obtained from the N_2 gas permeation measurements. The data are presented in Table II. Evidently, with the increase of EG loading, the nitrogen permeability of the nanocomposite reduces significantly.

A simple two-dimensional model developed by Nielsen[41] is widely used to predict the barrier performances of polymer composites containing sheet-structured fillers. The model is strictly based on tortuosity argument. It is further developed[42] with a view to the dependence of the tortuosity factor on the orientational order of the sheets in a continuous manner.

On the assumption that the orientation of the sheets is in a random mode, eq. (8) is used to model the dependence of the relative gas permeability on the EG volume fraction (Φ_f) and its aspect ratio ($2r/d$), where P is the gas permeability coefficient of the composite, and P_0 is that of the neat matrix.

$$P \Big/ P_0 = \frac{1 - \Phi_f}{1 + \left(r \Big/ d\right)\left(\Phi_f \Big/ 3\right)} \tag{8}$$

Figure 6 shows the relative N_2 permeability coefficient (P/P_0) of the nanocomposite as a function of the EG volume fraction. With the increase of the EG volume fraction, the nanocomposite shows a rapid decrease in gas permeability. In addition, the theoretical curve predicted by eq. (8) using an r/d value of 75 agrees well with the experimental data, indicating that the average aspect ratio ($2r/d$) of the EG sheets is about 150. By considering the fact that the orientation of the EG platelets is perpendicular to the direction of gas diffusion, which should benefit the gas barrier property, the actual average aspect ratio of EG in the nanocomposite may be smaller.

Comparing the calculated values of the aspect ratio from the mechanical tests and the gas barrier property tests, as indicated in Figure 6, we found a discrepancy in the calculated data of the aspect ratio of EG platelets based on the modified Nielsen model (with an approximate r/d value of 75) and the Halpin-Tsai model (with an approximate r/d value of 50). However, given that these two models are constructed to describe totally irrelevant physical properties, some systematic errors may arise from the models; and the modulus and density values of EG obtained from literatures are also the possible reasons for the observed discrepancy. Thereby, we considered such difference was acceptable. A brief estimation about the average aspect ratio of EG platelets in the nanocomposites prepared by LCM is in the range of 100–150.

Electrical Conductivity

As a conductive filler, the addition of EG is expected to improve the electrical conductivity of the composite. In our experiments,

Table II. Physical Properties of Neat ACM and EG/ACM Composites

Samples	Neat ACM	EG(5)/ACM	EG(10)/ACM	EG(10)/ACM
EG loading (phr)	0	5	10	10
Compounding method	-	LCM	LCM	Direct Blending
Density (gcm^{-3})	1.153 ± 0.002	1.182 ± 0.003	1.202 ± 0.005	1.193 ± 0.003
Apparent friction coefficient	1.2 ± 0.2	1.9 ± 0.3	1.4 ± 0.2	0.3 ± 0.1
Specific wear rate ($10^{-4}mm^3N^{-1}m^{-1}$)	7000 ± 3000	30 ± 10	9 ± 2	310 ± 10
Gas permeability coefficient ($10^{-17}m^2Pa^{-1}\ s^{-1}$)	4.05 ± 0.13	2.39 ± 0.08	1.75 ± 0.06	2.87 ± 0.09
Electrical conductivity[a] ($10^{-2}S\ cm^{-1}$)	0	1.70 ± 0.01	18.50 ± 0.06	0

[a]The electrical conductivity values are obtained from the EG/ACM coagulated compounds; the compounds lose the conductivity after milled on a miller.

the neat ACM and the EG/ACM composite prepared by direct blending were found to be electrically insulating. The EG/ACM compounds prepared by LCM exhibited certain electrical conductivities (data listed in Table II) as the coagulated compounds; however, they soon lost them when milled with the curing agent on the miller. Similar situations have been reported in our previous work.[31] This time, the observations to the Payne effect of the composites revealed the detailed changes in filler network.

Payne effect[43,44] is widely used to characterize filler dispersion and filler network in the filled rubber compounds. The Payne effect describes such a phenomenon that the storage modulus (G') of the filled rubber compound increases a lot at small strain amplitude compared with that of the neat rubber matrix, but decreases with increasing applied dynamic strain amplitudes. Some research suggest that the Payne effect should be attributed to the formation of filler network by both filler–filler interactions and filler–rubber interactions and the subsequent deconstruction of the filler network by increasing strain.

As showed in Figure 7, a dramatic decrease in G' is observed by comparing the EG/ACM coagulated compound and the milled compound, indicating that the EG network changed greatly before and after the milling shear force. We believe such dramatic change in the EG network shut off the electrical conductivity of the compound. Detailed stories in the filler network transformations during processing were described in another submitted work with the layered silicates.

CONCLUSIONS

A stable aqueous suspension of EG was obtained by dispersing microwave irradiation thermo-shocked expanded graphite into deionized water in the presence of surfactant SDS under ultrasonication. Well-performing EG filled ACM nanocomposites were obtained by a facile approach of latex compounding method. EG platelets were finely dispersed in the ACM matrix. The nanocomposites possessed greatly increased modulus and strength, together with improved wear resistance, and better gas barrier property. The coagulated EG/ACM compound exhibited

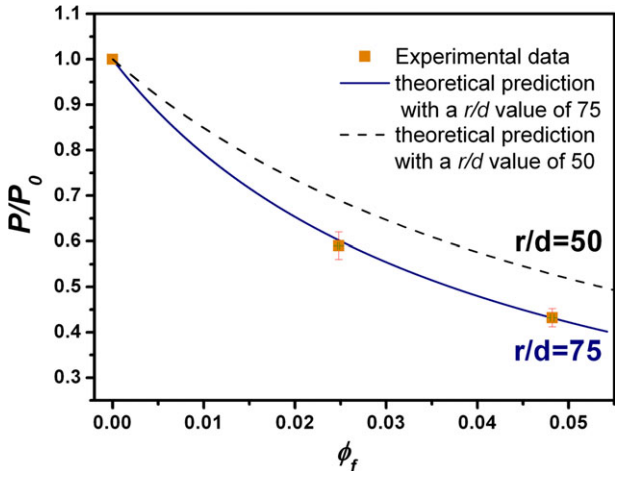

Figure 6. The dependence of relative gas permeability coefficient on EG volume fraction in the EG/ACM nanocomposites prepared by LCM, and theoretical predictions from the modified tortuosity-based model. [Color figure can be viewed in the online issue, which is available at wileyonlinelibrary.com.]

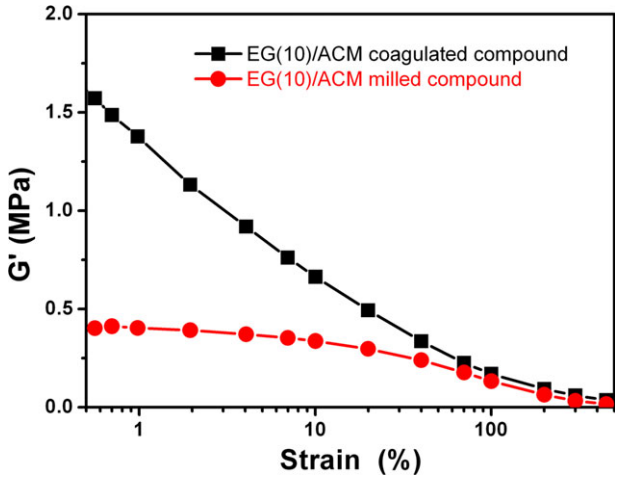

Figure 7. Strain amplitude dependence of storage modulus (G') of the EG(10)/ACM nanocomposite prepared by LCM in the state of coagulated compound and milled compound. [Color figure can be viewed in the online issue, which is available at wileyonlinelibrary.com.]

certain electrical conductivity, but lost it after milled on a miller. A dramatic change in EG network corresponded to the loss of electrical conductivity.

ACKNOWLEDGMENTS

This research is financially supported by the National Natural Science Foundation of China (50403029) and the National Natural Science Funding for Distinguished Young Scholars (50725310); the authors also acknowledge the Chang-Jiang Scholar program of the Ministry of Education, China (IRT0807).

REFERENCES

1. Allen, M. J.; Tung, V. C.; Kaner, R. B. *Chem. Rev.* **2010**, *110*, 132.
2. Geim, A. K. *Science* **2009**, *324*, 1530.
3. Terrones, M.; Botello-Méndez, A. R.; Campos-Delgado, J.; López-Urías, F.; Vega-Cantú, Y. I.; Rodríguez-Macías, F. J.; Elías, A. L.; Muñoz-Sandoval, E.; Cano-Márquez, A. G.; Charlier, J.-C.; Terrones, H. *Nano Today* **2010**, *5*, 351.
4. Kumar, A.; Zhou, C. *ACS Nano* **2010**, *4*, 11.
5. Potts, J. R.; Dreyer, D. R.; Bielawski, C. W.; Ruoff, R. S. *Polymer* **2011**, *52*, 5.
6. Kim, H.; Abdala, A. A.; Macosko, C. W. *Macromolecules* **2010**, *43*, 6515.
7. Kuilla, T.; Bhadra, S.; Yao, D.; Kim, N. H.; Bose, S.; Lee, J. H. *Prog. Polym. Sci.* **2010**, *35*, 1350.
8. Dreyer, D. R.; Park, S.; Bielawski, C. W.; Ruoff, R. S. *Chem. Soc. Rev.* **2010**, *39*, 228.
9. Geng, Y.; Wang, S. J.; Kim, J.-K. *J. Colloid Interface Sci.* **2009**, *336*, 592.
10. Sridhar, V.; Oh, I.-K. *J. Colloid Interface Sci.* **2010**, *348*, 384.
11. Yu, W. J.; Chae, S. H.; Perello, D.; Lee, S. Y.; Han, G. H.; Yun, M.; Lee, Y. H. *ACS Nano* **2010**, *4*, 5480.
12. Zhi, L.; Mullen, K. *J. Mater. Chem.* **2008**, *18*, 1472.
13. Hu, L.; Hecht, D. S.; Grüner, G. *Chem. Rev.* **2010**, *110*, 5790–5844.
14. Li, X.; Magnuson, C. W.; Venugopal, A.; An, J.; Suk, J. W.; Han, B.; Borysiak, M.; Cai, W.; Velamakanni, A.; Zhu, Y.; Fu, L.; Vogel, E. M.; Voelkl, E.; Colombo, L.; Ruoff, R. S. *Nano Lett.* **2010**, *10*, 4328.
15. Reynolds Iii, R. A.; Greinke, R. A. *Carbon* **2001**, *39*, 479.
16. Wakeland, S.; Martinez, R.; Grey, J. K.; Luhrs, C. C. *Carbon* **2010**, *48*, 3463.
17. Wei, T.; Fan, Z.; Luo, G.; Zheng, C.; Xie, D. *Carbon* **2009**, *47*, 337.
18. Rafiee, M. A.; Rafiee, J.; Srivastava, I.; Wang, Z.; Song, H.; Yu, Z. Z.; Koratkar, N. *Small* **2010**, *6*, 179.
19. Ramanujam, B. T. S.; Mahale, R. Y.; Radhakrishnan, S. *Compos. Sci. Technol.* **2010**, *70*, 2111.
20. Afanasov, I. M.; Morozov, V. A.; Kepman, A. V.; Ionov, S. G.; Seleznev, A. N.; Tendeloo, G. V.; Avdeev, V. V. *Carbon* **2009**, *47*, 263.
21. Zhao, X.; Zhang, Q.; Chen, D.; Lu, P. *Macromolecules* **2010**, *43*, 2357.
22. Villar-Rodil, S.; Paredes, J. I.; Martinez-Alonso, A.; Tascon, J. M. D. *J. Mater. Chem.* **2009**, *19*, 3591.
23. Xu, Z.; Gao, C. *Macromolecules* **2010**, *43*, 6716.
24. Li, J.; Sham, M. L.; Kim, J.-K.; Marom, G. *Compos. Sci. Technol.* **2007**, *67*, 296.
25. Debelak, B.; Lafdi, K. *Carbon* **2007**, *45*, 1727.
26. Sengupta, R.; Bhattacharya, M.; Bandyopadhyay, S.; Bhowmick, A. K. *Prog. Polym. Sci.* **2011**, *36*, 638.
27. Zhang, L.; Wang, Y.; Wang, Y.; Sui, Y.; Yu, D. *J. Appl. Polym. Sci.* **2000**, *78*, 1873.
28. Ma, J.; Xiang, P.; Mai, Y.-W.; Zhang, L.-Q. *Macromol. Rapid Commun.* **2004**, *25*, 1692.
29. Wu, Y.-P.; Wang, Y.-Q.; Zhang, H.-F.; Wang, Y.-Z.; Yu, D.-S.; Zhang, L.-Q.; Yang, J. *Compos. Sci. Technol.* **2005**, *65*, 1195.
30. Chung, D. D. L. *J. Mater. Sci.* **1987**, *22*, 4190.
31. Yang, J.; Zhang, L.-Q.; Shi, J.-H.; Quan, Y.-N.; Wang, L.-L.; Tian, M. *J. Appl. Polym. Sci.* **2010**, *116*, 2706.
32. Wang, L.; Zhang, L.; Tian, M. *Wear* **2012**, *276–277*, 85.
33. Bielinski, D.; Slusarski, L.; Janczak, K. J.; Loden, A. *Wear* **1993**, *169*, 257.
34. Yang, J.; Tian, M.; Jia, Q.-X.; Zhang, L.-Q.; Li, X.-L. *J. Appl. Polym. Sci.* **2006**, *102*, 4007.
35. Fornes, T. D.; Paul, D. R. *Polymer* **2003**, *44*, 4993.
36. Hsueh, C.-H. *Compos. Sci. Technol.* **2000**, *60*, 2671.
37. Affdl, J. C. H.; Kardos, J. L. *Polym. Eng. Sci.* **1976**, *16*, 344.
38. Chung, D. *J. Mater. Sci.* **2002**, *37*, 1475.
39. Stankovich, S.; Dikin, D. A.; Dommett, G. H. B.; Kohlhaas, K. M.; Zimney, E. J.; Stach, E. A.; Piner, R. D.; Nguyen, S. T.; Ruoff, R. S. *Nature* **2006**, *442*, 282.
40. Lee, C.; Wei, X.; Li, Q.; Carpick, R.; Kysar, J. W.; Hone, J. *Phys. Status Solidi B* **2009**, *246*, 2562.
41. Nielsen, L. E. *J. Macromol. Sci., Part A* **1967**, *1*, 929.
42. Bharadwaj, R. K. *Macromolecules* **2001**, *34*, 9189.
43. Payne, A. R. *J. Appl. Polym. Sci.* **1962**, *6*, 57.
44. Allegra, G.; Raos, G.; Vacatello, M. *Prog. Polym. Sci.* **2008**, *33*, 683.